Optimal Operation of Rotor-Wing Assemblies on eVTOL Aircraft

Jonah Whitt
PhD Student

Farhan Gandhi
Redfern Professor and MOVE Director

Center for Mobility with Vertical Lift (MOVE)
Rensselaer Polytechnic Institute
Troy, New York, United States

ABSTRACT

eVTOL aircraft with tilting rotors and fixed wings for cruise lift have control redundancy leading to the possibility of optimal operation over the range of airspeeds. In this study, a single rotor-wing unit is considered to examine how a combination of rotor RPM, rotor root pitch, rotor cant, and wing angle of attack can minimize the power requirement, while ensuring that the rotor-wing unit provides the necessary lifting and propulsive forces. Analysis is conducted for both a UAV-scale rotor-wing unit producing 5 lbs lift as well as a manned-UAM scale unit producing 550 lbs lift. For both cases, the power requirements are highest in hover, reduce rapidly as airspeed increases, and then increase slowly at speeds greater than maximum endurance speed. For minimum power operation, the rotors are oriented mostly up at low speed with a relatively low root pitch setting of 25-30 deg, and fully forward (operating as axial propellers) at speeds greater than maximum endurance speed, with the root pitch increasing significantly to account for axial flow through the rotor. At speeds right before the rotor starts tilting downward, the wing lift-share is ~25%, increasing to ~83% at maximum endurance speed, and 100% at higher cruise speeds. If the rotor solidity is low (similar to a UAV-scale propeller, and not high as seen on manned-UAM scale eVTOL rotors), it is feasible to use a fixed pitch rotor set at optimal low-speed values. For such low-solidity fixed-pitch rotors, the power penalty at cruising speeds may be acceptable, but the rotors must operate in a tilted position, rather than oriented fully forward like axial propellers.

INTRODUCTION

eVTOL companies over the last 10–15 years have experimented with various aircraft configuration-types (e.g., Refs. 1–11). While these have included configurations relying on *pure rotor-borne lift* (e.g., EHang184 and EHang216, Vertical Aerospace VA-X2, and Boeing's Cargo Air Vehicle), a large number of eVTOL aircraft are using the efficiency of *wing-borne lift in cruise*, especially aircraft with larger payload and range requirements. The aircraft relying on wing-borne lift can further be classified into two major categories: those using *lift plus cruise*, where the lifting rotors stow, and a dedicated propeller and wing are utilized in cruise (e.g., Boeing Passenger Air Vehicle, Wisk's Gen-5 Cora, and Beta Technologies' Alia-250, see Fig. 1); and those using *tilting prop-rotors*, where dedicated propulsors are eschewed, and some or all of the lifting rotors are tilted forward to provide propulsive thrust in combination with wing-borne lift, in cruise. (e.g., Archer Aviation's Midnight, Wisk's Gen-6, Joby Aviation's S4, and Vertical Aerospace's VA-X4, see Fig. 2). Among eVTOL configurations for air-taxi application, the tilting prop-rotor configuration appears to be one that several manufacturers are favoring for further development toward certification.

Fig. 1: "Lift plus cruise" eVTOL configurations

Presented at the Vertical Flight Society's 79th Annual Forum & Technology Display, West Palm Beach, FL, USA, May 16-18, 2023.

Fig. 2: eVTOL configurations using tilting prop-rotors

For eVTOL aircraft with tilting prop-rotors, the availability of control redundancy offers multiple ways of flying the aircraft, and leads to the question of determining the optimal trim over the range of airspeeds. The rotors, for example, can be operating at different rotational speeds, different root pitch settings, and different tilt orientations (or cant angles). The aircraft pitch attitude can similarly be adjusted to generate varying amounts of lift from the wings. The combination of rotors and wing on the eVTOL aircraft must generate the necessary lift and propulsive force required at any operating condition, but how the rotors and wing collaborate to do so, in addition to equilibrating the other forces and moments, merits close examination, and provides inspiration for this study. Similar studies have previously been carried out examining the use of redundant controls on high-speed compound and coaxial helicopters to minimize power requirement, vibration, or noise (e.g., Refs 12–15). Instead of using a specific eVTOL aircraft configuration as the basis, the present study focuses on a typical single rotor-wing unit (see for example, the unit marked in red in Fig. 3) in an attempt to expand the study's generality. Thus, the learnings from this study could apply to eVTOL aircraft with different numbers of rotors (6 for Joby S4, 8 for Vertical VA-X4, and 12 for Archer Midnight and Wisk Cora, as seen in Fig. 2).

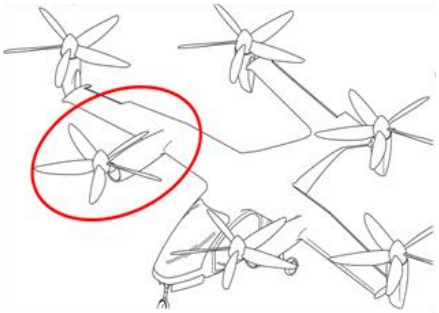

Fig. 3: Single tilting rotor and wing unit of an eVTOL aircraft

The current study focuses on *optimal operation of a single rotor-wing unit* to maximize performance over an operational airspeed range. In particular, if the rotor and wing designs are established, what should the rotor speed and root pitch setting be, what should the rotor cant angle (the tilt of the rotor's rotational axis relative to the wing chordline) be, and what should the aircraft pitch attitude be over the operating envelope? The goal in the present study is to minimize power requirement, while understanding in detail how the system works when performing optimally at various operating conditions. The rotor-wing units are sized to represent aircraft at two different scales, a 20 lbs UAV and a 3,300 lbs UAM-scale vehicle for human transportation. The study also considers the feasibility of using fixed-pitch rotors and examines power penalty and operational differences compared to the case with variable pitch rotors, and considers the role of rotor solidity with regard to this question.

MODELING

Setup and Parameterization

In this paper, a single rotor-wing section was used for studies at both the small (UAV) scale as well as the large (manned-UAM) scale. This single rotor-wing section includes a full rotor and a wing section with a span length of 2.2R (where R is the rotor radius). Figure 4 exemplifies this wing and rotor section. To broaden the generality of the study, the rotor and wing are assumed to be isolated, and any rotor-wing interactions (which would be configuration-specific) are ignored. With this assumption, specifications such as geometric offsets of the rotor relative to the wing are not required. The geometries of the rotor and wing sections can themselves be varied, to analyze different configurations, at different scales.

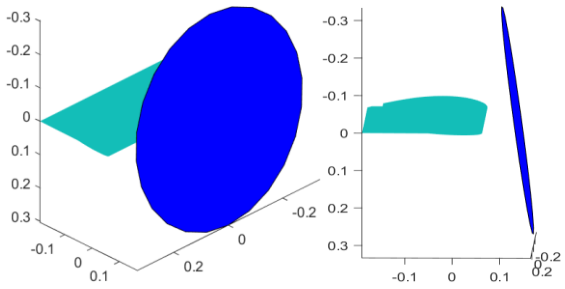

Fig. 4: Isometric and side views of rotor and wing section

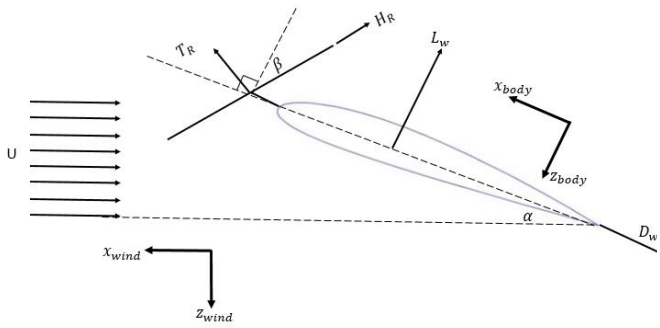

Fig. 5: Geometric parameterization of the rotor and wing section

Figure 5 shows two geometric parameters that characterize the system: the wing angle of attack, α; and the rotor cant angle, β, (representing the angle between the rotor's thrust axis and the wing's chord line). A cant angle of 0 deg represents a rotor operating as an axial propeller, whereas a cant angle of 90 deg represents a lifting rotor tilted fully upward. Furthermore, the section's "body" reference frame is aligned with the wing's chord line, with "L_W" and "D_W" the wing lift and drag in the body reference frame. Similarly, "T_R" and "H_R" are rotor thrust and drag in the rotor's reference frame. In the current analysis both rotor and wing forces are transformed into a common wind reference frame for force equilibrium considerations. Thus, in the wind reference frame, lift "L" generated by the rotor and wing, propulsive thrust "T" provided by the rotor, and section drag "D" that the rotor propulsive thrust must overcome are given as:

$$L = L_w \cos\alpha - D_w \sin\alpha + T_R \sin(\beta + \alpha) + H_r \cos(\beta + \alpha) \quad (1)$$

$$T = T_R \cos(\beta + \alpha) \quad (2)$$

$$D = \frac{D_{fus}}{\#\ of\ sections} + D_w \cos\alpha + L_w \sin\alpha + H_r \sin(\beta + \alpha) \quad (3)$$

This setup gives 4 trim/control variables for the wing and rotor section: rotor speed Ω, root pitch θ_R, rotor cant angle β, and wing angle of attack α. To obtain results, θ_R and β are parametrically varied, then the equilibrium equations $L = Weight/(\#\ of\ sections)$ and $T = D$, are solved to evaluate Ω and α. In the above equations, "# of sections" refers to number of rotor-wing units on the aircraft (for e.g., 6 on the Joby S4 aircraft).

Platform Details

For analysis at the UAV-scale, the DEVCOM Army Research Laboratory's 20 lb. QuadRotor Tail Sitter (Fig. 6) was used as starting point-of-reference (Ref. 16). Key wing, rotor, and fuselage properties are shown in Table 1, with additional details in Ref. 16. The rotor has a NACA4412 airfoil section at the root a ClarkY airfoil at the tip. Airfoil data is interpolated between the root and tip. The wing section has a span of 2.2R and uniformly uses the Wortmann FX-63-137 airfoil section. Fuselage forces come from a determined flat-plate drag area of 0.015 m^2 (Ref. 16). As the 20 lbs QuadRotor Tail Sitter has 4 rotor-wing units, the "# of sections" is 4. A single rotor-wing unit is then required to produce 5 lbs lift, and also overcome one fourth of the fuselage drag. Note that although rotor-wing properties are "borrowed" from the QuadRotor Tail Sitter, the notional UAV-scale eVTOL aircraft being analyzed in this study is *not* a tail-sitter, where the whole aircraft pitches forward in cruise. Instead, rotor tilting is allowed. Additionally, the presence of rotor pitch variation further distinguishes the aircraft considered in the present study from the point-of-departure QuadRotor Tail Sitter configuration.

Fig. 6: DEVCOM ARL 20lb QuadRotor Tail Sitter

For analysis at the manned-UAM scale, the rotor and wing models for the UAV-scale aircraft are scaled up for a 3,300 lbs eVTOL aircraft. The geometric properties for this larger aircraft are also given in Table 1. While blade twist, rotor and wing airfoils are identical to those for the UAV-scale aircraft, one key difference is that the rotor solidity is much larger, and more representative of manned-scale eVTOL aircraft currently in development. Fuselage drag for this notional aircraft is estimated by scaling the fuselage drag of the lift+cruise NASA concept vehicles described in Ref. 17. This aircraft is assumed to have 6 tilting rotors along the wing span ("# of sections" is 6), so each rotor wing unit has to generate 550 lbs lift, equivalent to one sixth of the aircraft weight, and the propulsive force generated by the unit must also overcome one sixth of the fuselage drag. Effects of hover-only/stowed aft-rotors (such as seen on Archer Midnight, Wisk Gen6, and Vertical VA-X4) are not considered in this study.

Table 1. Small and Large Scale Section Properties

Characteristic	Small Scale	Large Scale
Rotor Diameter	2 ft	6 ft
Rotor Solidity	0.060	0.265
Fuselage D/q	0.161 ft^2	1.29 ft^2
Gross Weight	20 lb	3300 lb
Wing Chord	5/6 ft	3 ft

eVTOL Analysis Model (RMAC)

Aircraft trim analysis was conducted using the Rensselaer Multicopter Analysis Code (RMAC), a physics-based state model for electric VTOL aircraft (details in Ref. 18). For this study, RMAC predicts rotor forces using a 10-state Peters-He inflow model for each rotor. Wing forces are predicted with a fixed-wing model based on lifting-line theory described by Anderson (Ref. 19). Furthermore, as the rotor-wing section can be anywhere along the vehicle, any effects of wing-tip vortices are ignored.

RESULTS

20 lb Unmanned Aircraft

As noted in the Analysis section, there are four trim parameters: rotor speed Ω, root pitch θ_R, rotor cant angle β, and wing angle of attack α. At any airspeed, $\theta_R$and β are parametrically varied, and Ω and α are then evaluated by solving for force equilibrium in the horizontal (wind) and vertical (gravity) directions. By examining the results over the variations in θ_R and β, the minimum power, and the trim parameters corresponding to this minimum power states, can be determined at any airspeed. Figure 7 shows the variation in minimum required power at any airspeed, versus airspeed, and Figs 8a–8c show corresponding variations in β, α, Ω, and θ_R, respectively. From Fig.7, maximum endurance speed is observed to be 25 kts, and the airspeed corresponding to best range lies between 25–30 kts. For minimum power operation, from Fig. 8a the rotor is observed to be oriented mostly upward (cant angle of 80 deg) up to a speed of 15 kts, and forward (cant angle of 0 deg) at speeds greater than 25 kts, with transition between 15–25 kts. Also in Fig. 8a, the wing angle of attack is between 8–10 deg at low speeds (under 15 kts). As the rotor starts tilting forward at speeds greater than 15 kts, the wing is set at a high angle (~14 deg) to maximize its lifting capability, with this angle progressively decreasing as the airspeed increases. The rotor RPM (Fig. 8b) generally follows the power curve, with the RPM being high in hover and at low speeds, when the rotor is providing lift. With the availability of wing lift in transition and cruise, the rotor RPM is observed to be lower. Figure 8c shows the variation in rotor pitch with airspeed, for minimum power operation. At low speeds, when the rotor is primarily lifting, the root pitch is set relatively low (25 deg), and at high speed when the rotor is generally operating as an axial propeller, the root pitch is set high (60 deg), with the pitch increasing between the two values over the 25–35 kts speed range.

A more detailed analysis is carried out at hover, 15 kts (transition), 25 kts (max endurance), and 35 kts (high-speed cruise) conditions, and these cases are discussed below. In hover, the rotor points vertically up, so the sum $\alpha + \beta = 90\ deg$. At low pitch values, θ_R, the rotor is required to operate at higher Ω to generate the necessary lift and this results in an increase in power. At high θ_R rotor stall and an associated increase in rotor profile drag similarly increases power. Through parametric variation studies, the optimal root pitch was determined to be ~25 deg, with a corresponding operational speed of 2610 RPM in hover. Figure 9 and Figs. 10a–10d present results at 15 kts, as functions of root pitch and cant angle. The minimum power point is shown on each of the figures as a red marker. On Fig. 9, the minimum power point corresponds to a θ_R of 25 deg and a β of 80 deg, consistent with the results previously seen on Figs. 6a and 6d. On Fig. 10a, the minimum power point lies within low RPM sections on the β– θ_R map. From Figs. 10b and 10c it is observed that for minimum power, the wing operates at an angle of attack of under 10 deg, and generates a lift of 1.2 lbs (out of a total of 5 lbs, or 24% lift share). Figure 10d shows the total section drag (Eq. 3), and at the optimal operating point, the total drag is observed to be very low. Operating at high rotor pitch or low rotor cant angles (rotor approaching propeller mode) at 15 kts airspeed is undesirable. High rotor pitch, in the absence of a large axial flow component results in rotor stall and substantially increased rotor power. Low rotor cant angle (relative to the wing chordline) necessitates higher wing angles of attack to orient the rotor thrust upward, and this in turn results in high wing drag (which contributes to increased total drag, see Fig. 10d).

Figure 11 and Figs. 12a–12d present similar results at 25 kts. On Fig. 11, the minimum power point corresponds to a θ_R of 35 deg and a β of 50 deg, consistent with the results previously seen on Figs. 8a and 8c. On Fig. 12a, the minimum power point again lies within low RPM section on the β– θ_R map. From Figs. 12b and 12c it is observed that for minimum power, the wing operates at an angle of attack of around 12 deg, and generates a lift of 4.15 lbs (out of a total of 5 lbs, or 83% lift share). Figure 12d shows the total section drag (Eq. 3) at the optimal operating point is close to the lowest values calculated. Returning to Fig. 12b, it is noted that at 25 kts, the wing is incapable of producing the entirety of the required 5 lbs lift. Setting the rotor at an intermediate tilt, then, effectively supplements the wing lift and simultaneously provides the required propulsive forced. If the cant angle is set too low (rotor predominantly in propeller mode), the rotor is unable to simultaneously meet its lifting and propulsive force requirements efficiently. To provide the required lifting component at low cant angles, there is a simultaneous increase in net rotor thrust (results not shown) and an increase in wing angle of attack (Fig. 12c). At cant angles lower than 40 deg, the high wing angle of attack puts it in a post stall condition, resulting in high wing drag (which results in increased total drag, see Fig. 12d).

Figure 13 and Figs. 14a–14d present a comprehensive set of results at 35 kts. On Fig. 13, the minimum power point corresponds to a θ_R of 55 deg and a β of 0 deg (rotor oriented forward in propeller mode), consistent with the results previously seen on Figs. 8a and 8c. On Fig. 14a, the minimum power point corresponds to operation at relatively low RPM values on the β– θ_R map, although not at the absolute minimum values. From Figs. 14b and 14c it is observed that for minimum power, the wing operates at an angle of attack of around 3 deg, and provides almost the entire lift. Operating

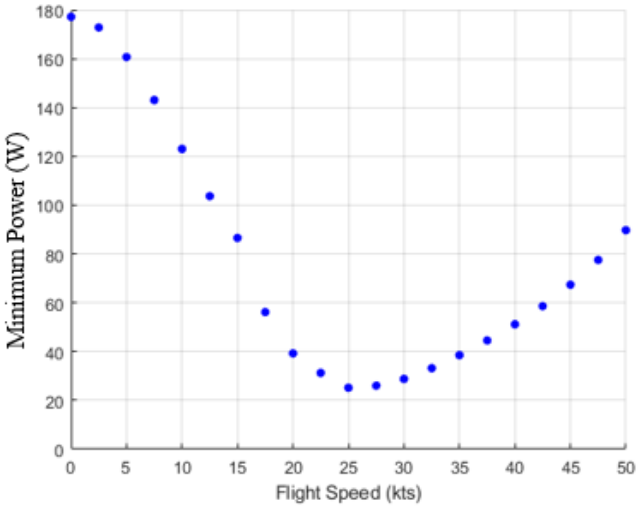

Fig. 7: Minimum rotor power vs flight speed

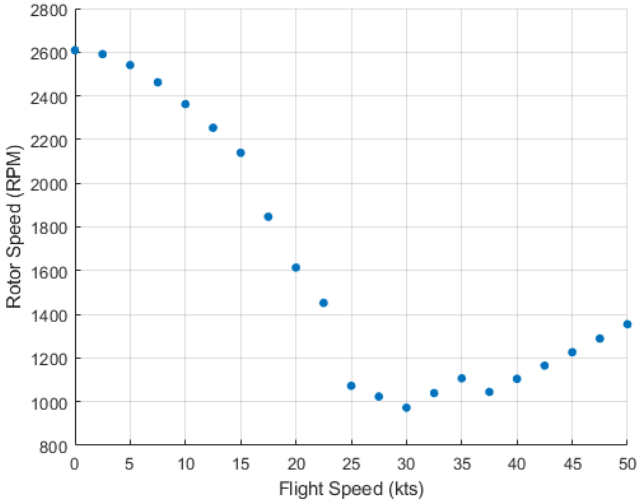

Fig. 8b: Rotor speed vs flight speed at minimum power

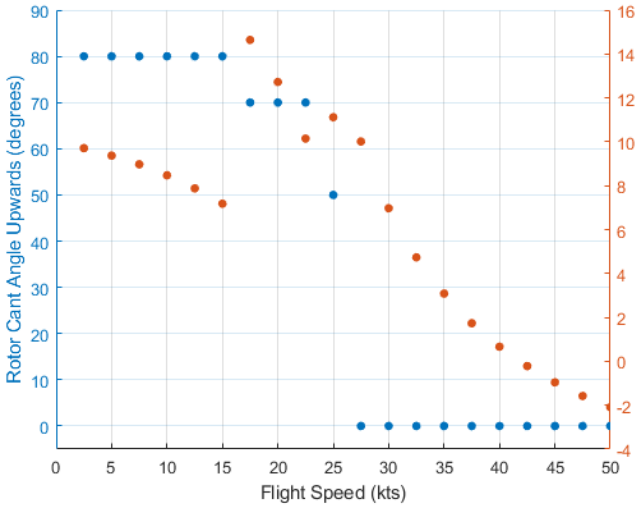

Fig. 8a: Rotor cant angle and wing angle of attack vs flight speed at minimum power

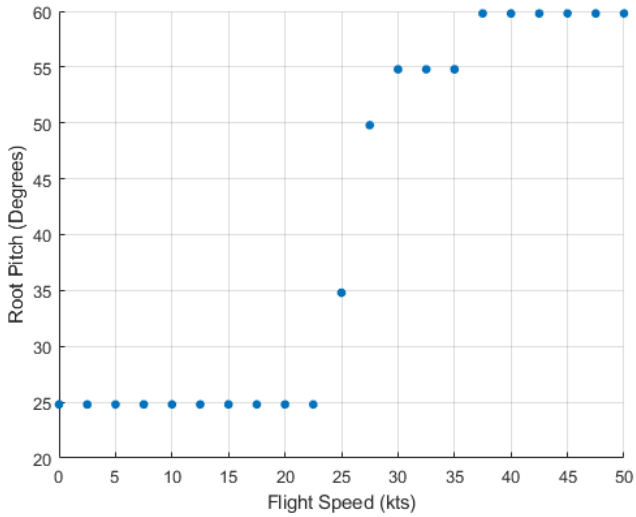

Fig. 8c: Rotor root pitch vs flight speed at minimum power

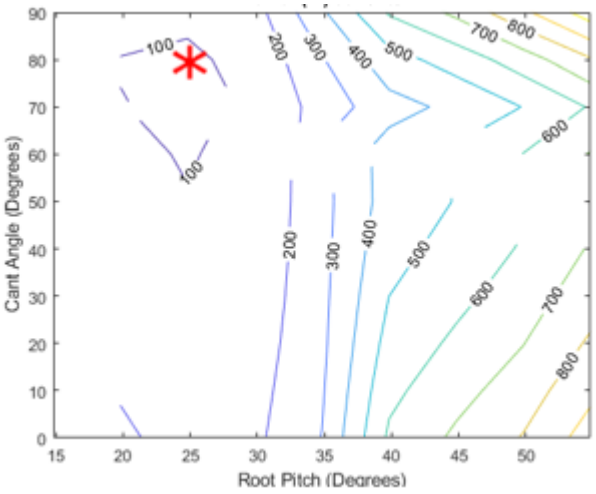

Fig. 9: Rotor power (W) with parametrically varied root pitch and rotor cant angle at 15 kts

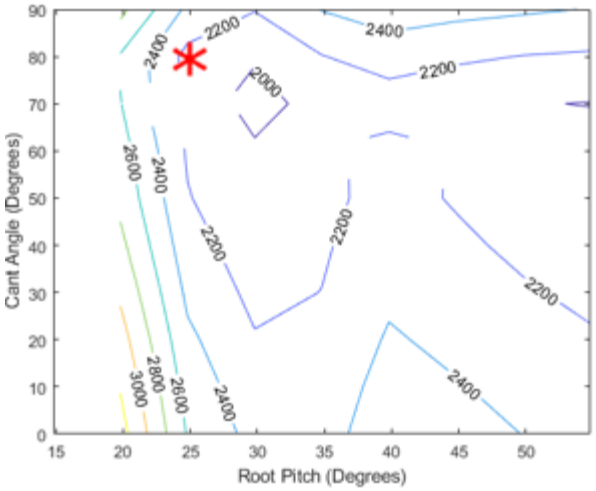

Fig. 10a: Rotor speed (RPM) with parametrically varied root pitch and rotor cant angle at 15 kts

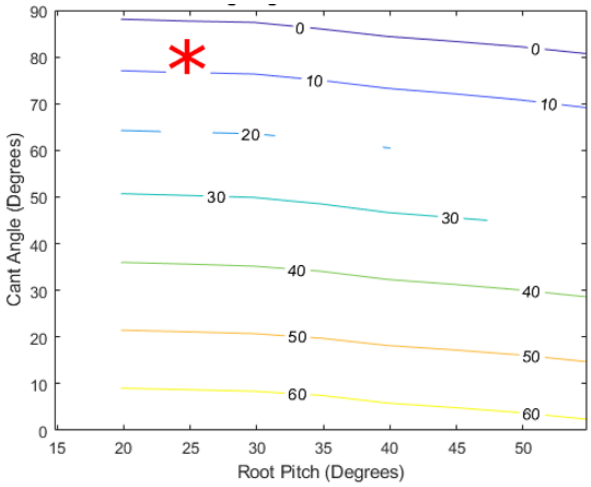

Fig. 10c: Wing angle of attack (deg) with parametrically varied root pitch and rotor cant angle at 15 kts

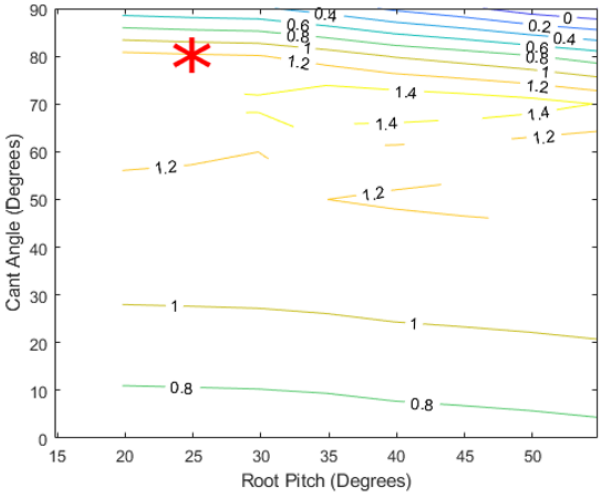

Fig. 10b: Wing lift (lb) with parametrically varied root pitch and rotor cant angle at 15 kts

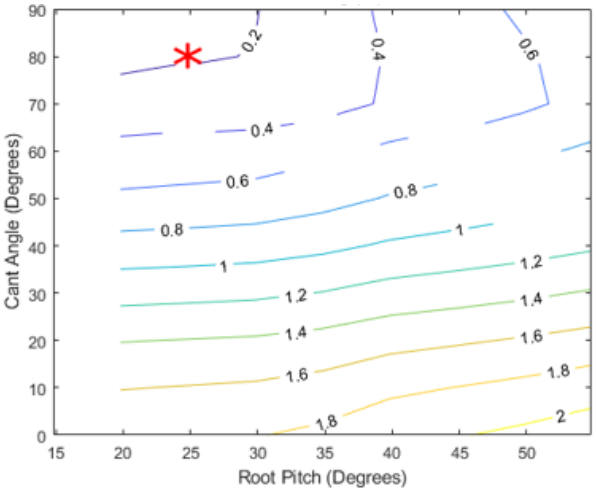

Fig. 10d: Section drag (lb) with parametrically varied root pitch and rotor cant angle at 15 kts

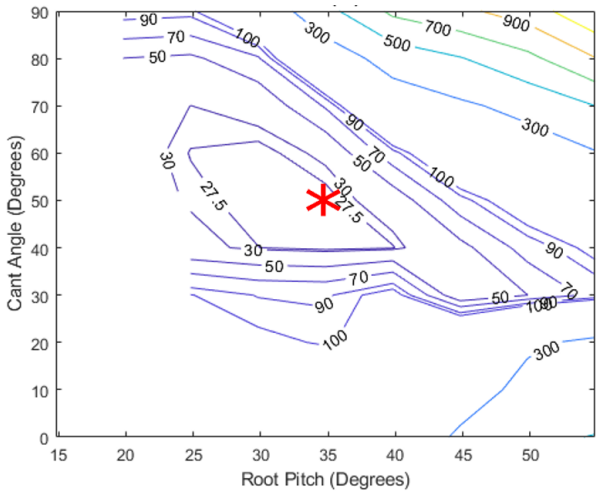

Fig. 11: Rotor power (W) with parametrically varied root pitch and rotor cant angle at 25 kts

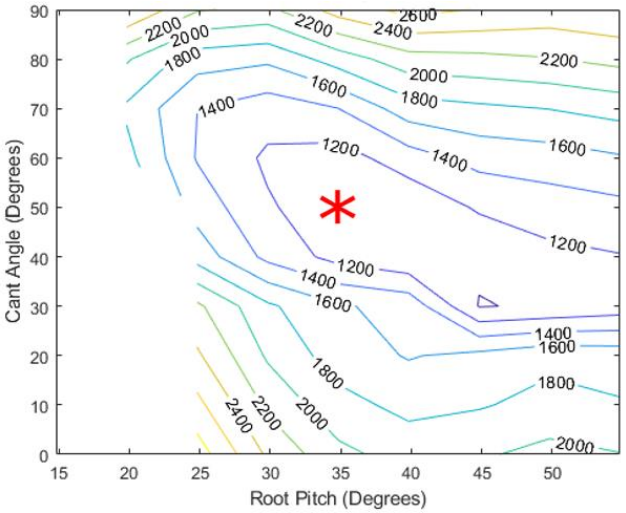

Fig. 12a: Rotor speed (RPM) with parametrically varied root pitch and rotor cant angle at 25 kts

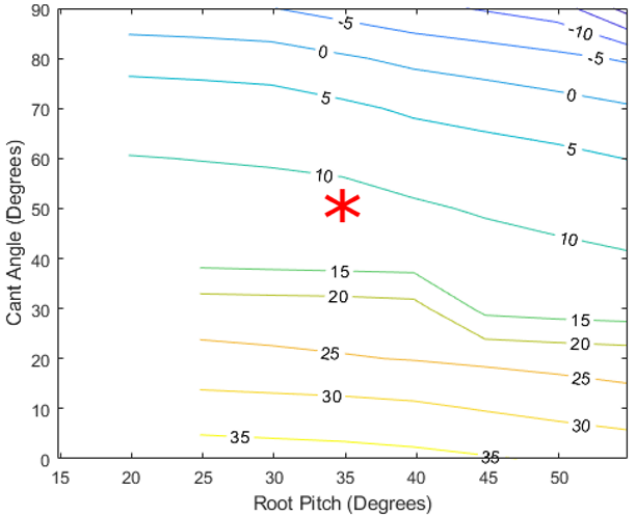

Fig. 12c: wing angle of attack (deg) with parametrically varied root pitch and rotor cant angle at 25 kts

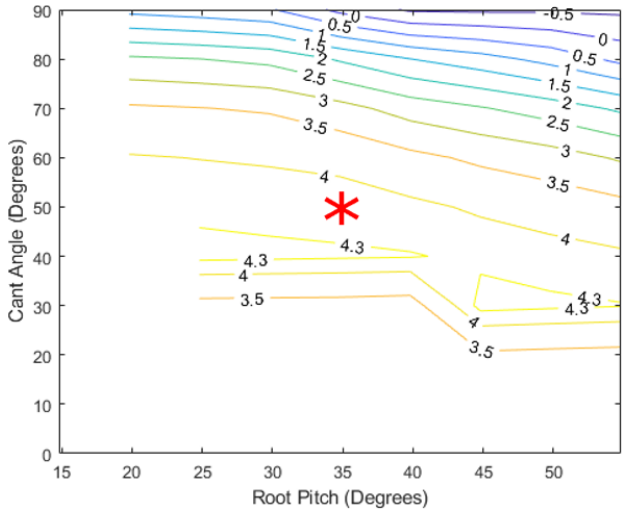

Fig. 12b: Wing lift (lb) with parametrically varied root pitch and rotor cant angle at 25 kts

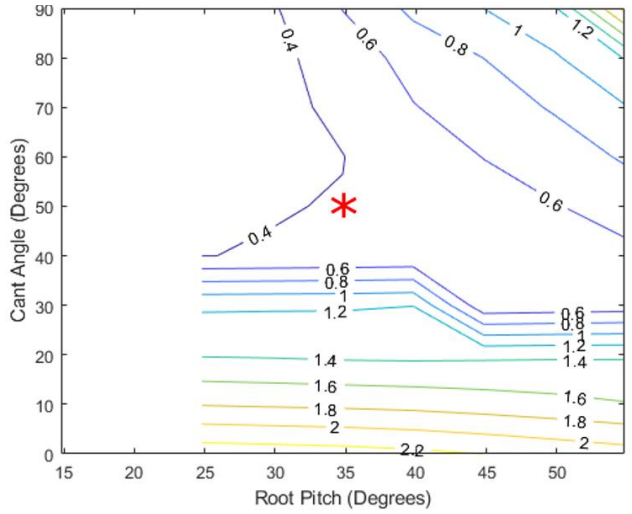

Fig. 12d: Section drag (lb) with parametrically varied root pitch and rotor cant angle at 25 kts

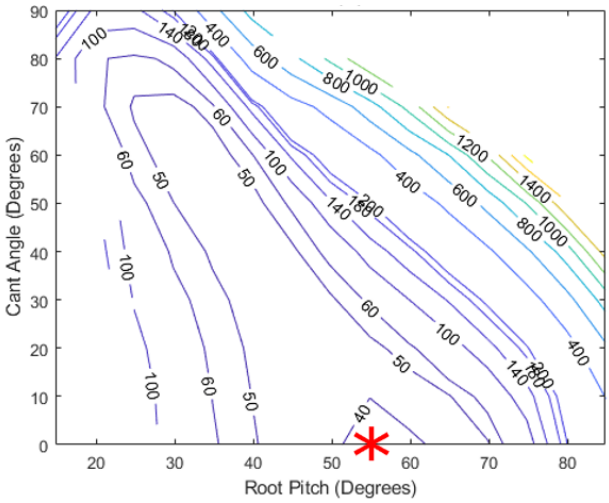

Fig. 13: Rotor power (W) with parametrically varied root pitch and rotor cant angle at 35 kts

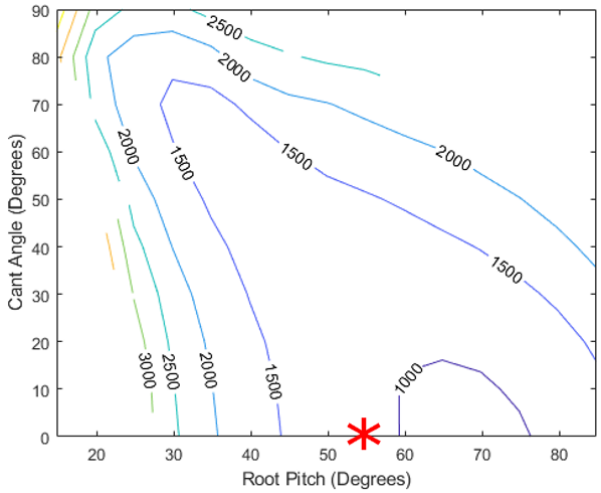

Fig. 14a: Rotor speed (RPM) with parametrically varied root pitch and rotor cant angle at 35 kts

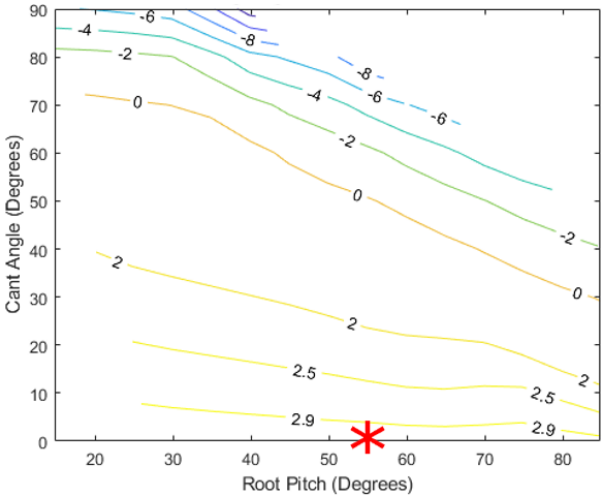

Fig. 14c: Wing angle of attack (deg) with parametrically varied root pitch and rotor cant angle at 35 kts

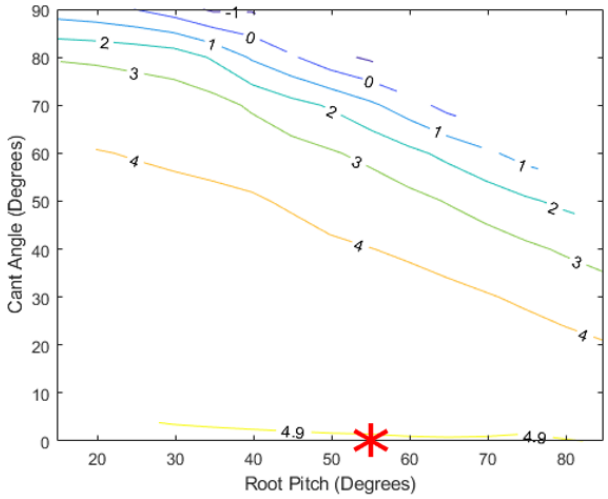

Fig. 14b: Wing lift (lb) with parametrically varied root pitch and rotor cant angle at 35 kts

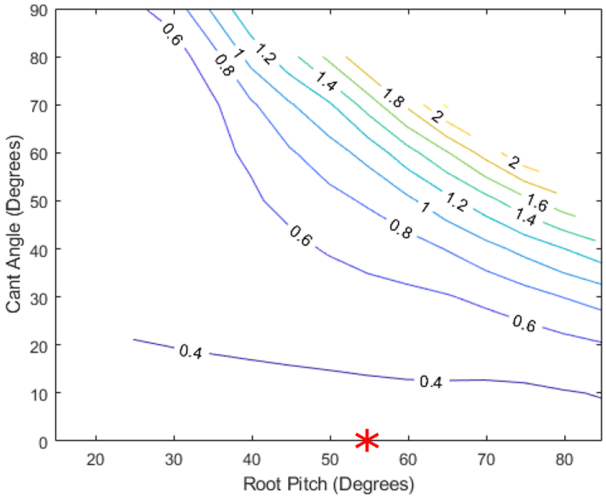

Fig. 14d: Section drag (lb) with parametrically varied root pitch and rotor cant angle at 35 kts

optimally at zero cant angle and low wing angle of attack results in low section drag (Eq. 3), as seen in Fig. 14d. At 35 kts, if the rotor cant angle is increased so the rotor is now providing some lift, the wing angle of attack needs to correspondingly reduce (Fig. 14c) to reduce wing lift contribution (Fig. 14b). Since rotor-borne lift is energetically much more expensive than wing borne lift, total power requirements would correspondingly increase, with increasing rotor cant (Fig. 13).

While the above results allowed variation in rotor speed and root pitch, rotor cant and wing angle of attack, one of the questions of interest in this study is whether it may feasible to use fixed pitch rotors, and what performance penalty that may entail. Figure 15 shows minimum power versus flight speed for variable pitch as well as several values of fixed root pitch.

The variable pitch results (open circles on Fig. 15) are the same as those previously seen in Fig. 7, and the corresponding optimal pitch variation was shown in Fig. 8c. Note that on Fig. 8c the optimal pitch was 25 deg for speeds lower than 25 kts, increasing to 55 deg for speeds between 30–35 kts, and to 60 deg at speeds beyond 35 kts. On Fig. 15 a fixed 25 deg root pitch has identical power requirement to variable pitch case for speeds below 25 kts (as expected), and increases only slightly, at higher speeds. Higher rotor pitch settings are favored at higher speeds to account for the axial flow component through the rotor. On Fig. 15, fixed root pitch values of 30 and 35 deg result in lower power requirement than a fixed root pitch of 25 deg for speeds greater than 25 kts, but these high pitch settings are detrimental at lower flight speeds since the rotor stalls. A lower fixed pitch setting of 20 deg performs worse than the 25 deg fixed pitch setting case over the entire airspeed range. From the above results, a fixed pitch setting of 25 deg could be a good choice if the desired operating range of the aircraft was 0–35 kts, with the aircraft very rarely venturing to higher speeds. At speeds under 25 kts, the 25 deg pitch setting is optimal. At 35 kts the power requirement is for 25 deg pitch is 48.5 W as compared to 38.5 W for the variable pitch rotor, corresponding to a 26% increase. The best range airspeed lies between 25–30 kts, and over this range, the average power penalty of using a 25 deg fixed pitch rotor is a 17% increase, relative to the variable pitch rotor operating optimally. Figures 16a–16b show the optimal rotor cant, wing angle of attack, and rotor RPM, for the 25 deg fixed pitch case (similar to Figs. 8a–8b for the variable pitch case). The most interesting observation from a comparison of Figs. 8 and 16 is that with a fixed 25 deg root pitch, the aircraft must operate at a high cant angle even in cruise, whereas for the variable pitch case the rotor cant angle reduces to zero and the rotor operates as an axial propeller in cruise. Specifically, from Fig. 16a, at speeds of 30 kts and higher, the rotor cant angle is seen to be 70 deg, so the rotor is tilted substantially (even mostly) upward. For the 25 deg fixed pitch case, at 35 kts, the rotor provides 28% of the total lift share (the wing is at 0 deg, Fig. 16a, compared to ~3 deg for the variable pitch case, Fig. 8a, where it provided all the required lift, Fig. 14b), and the rotor operating speed is about 1700 RPM, Fig. 16b (as opposed to 1150 RPM for the variable pitch case in Fig. 8b).

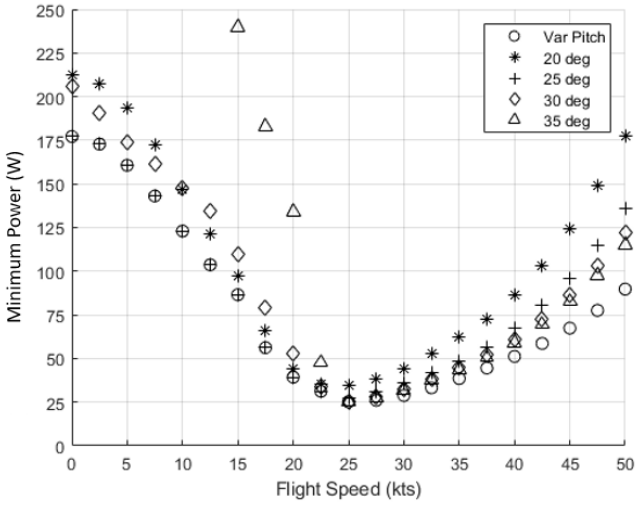

Fig. 15: Minimum power vs flight speed for fixed and variable pitched rotors

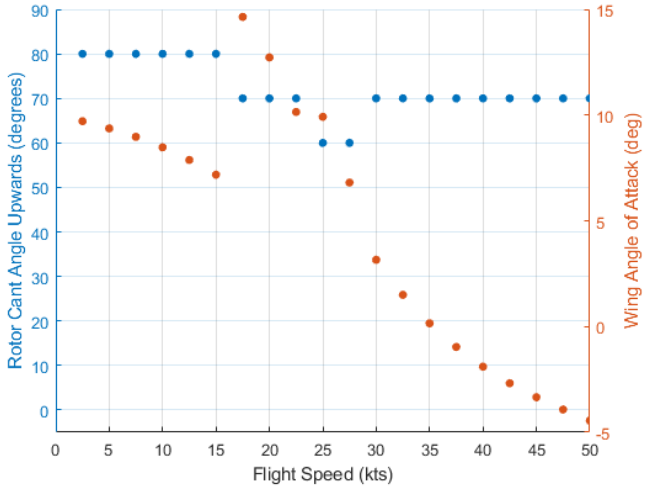

Fig. 16a: Rotor cant angle and wing angle of attack vs flight speed at minimum power, $\theta_R = 25°$

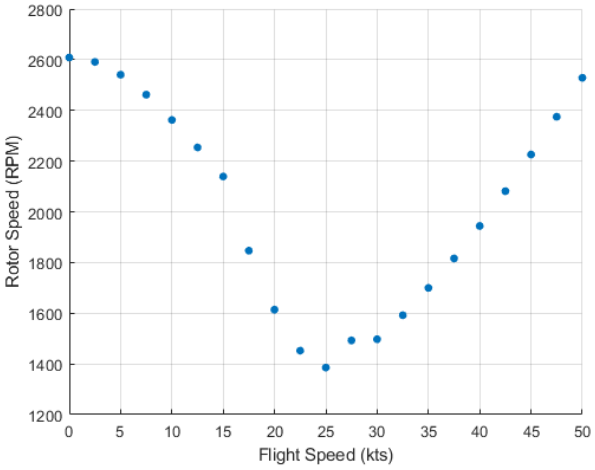

Fig. 16b: Rotor speed vs flight speed at minimum power, $\theta_R = 25°$

3,300 lb Aircraft (for Human Transport)

In this section, results for the 3,300 lbs aircraft are presented and discussed. As previously noted in the Analysis section it is assumed that the aircraft has 6 rotor/wing units, so each unit is required to produce 550 lbs lift Figure 17 shows the variation in minimum required power at any airspeed, versus airspeed, and Figs 18a–18c show corresponding variations in β, α, Ω, and θ_R, respectively. From Fig. 17, maximum endurance speed is observed to be 80–90 kts, and the airspeed corresponding to best range lies between 100–110 kts. For minimum power operation, from Fig. 16a the rotor is observed to be oriented mostly upward (cant angle of 70–80 deg) up to a speed of 60 kts, and forward (cant angle of 0 deg) at speeds greater than 80 kts, with transition between 60–80 kts. At speeds greater than 60 kts when the rotors start to tilt forward, the wing has to start contributing to lift generation. Also in Fig. 18a, at speeds of 60–80 kts, the wing is set at a high angle (12–13 deg) but the wing angle of attack progressively decreases as the airspeed increases. The rotor RPM (Fig. 18b) generally follows the power curve, with the RPM being high in hover and at low speeds when the rotor is providing lift. With the availability of wing lift in transition and cruise, the rotor RPM decreases significantly. Figure 18c shows the variation in rotor pitch with airspeed, for minimum power operation. At low speeds, when the rotor is primarily lifting, the root pitch is set relatively low (30 deg), and at high speed when the rotor is generally operating as an axial propeller, the root pitch is set high (85 deg), with the pitch increasing between these values over the 70–110 kts speed range.

A more detailed analysis is carried out at hover, 40 kts (transition), 80 kts (max endurance), and 120 kts (high-speed cruise) conditions, and these cases are discussed below. In hover, the rotor points vertically up, so the sum $\alpha + \beta = 90\ deg$. Through parametric variation studies, the optimal root pitch was determined to be ~30 deg, with a corresponding operational speed of 1560 RPM. As was the case for the 20 lbs aircraft, further reducing the pitch results in increase in rotor RPM requirements while increasing the pitch results in sections of the rotor stalling, both of which increase drag and power requirements.

Figure 19 and Figs. 20a–20d present results at 40 kts, as functions of root pitch and cant angle. The minimum power point is shown on each of the figures as a red marker. On Fig. 20, the minimum power point corresponds to a θ_R of 30 deg and a β of 70 deg, consistent with the results previously seen on Figs. 18a and 18c. On Fig. 20a, the minimum power point lies within low RPM sections on the β– θ_R map. From Figs. 20b and 20c it is observed that for minimum power, the wing operates at an angle of attack of around 14 deg, and generates a lift of 140 lbs (out of a total of 550 lbs, or ~25% lift share). Figure 20d shows the total section drag (Eq. 3). At the optimal operating point, the total drag is observed to be the lowest over the range of parameter variations considered. Operating at higher rotor pitch values at 40 kts airspeed is undesirable. With the rotor canted mostly upward, a high rotor pitch results in rotor stall and substantially increased rotor power in the absence of a large axial flow.

Figure 21 and Figs. 22a–22d present similar results at 80 kts (max endurance speed). On Fig. 21, the minimum power point corresponds to a θ_R of 50 deg and a β of 20 deg, consistent with the results previously seen on Figs. 18a and 18c. On Fig. 22a, the minimum power point again lies within low RPM section on the β– θ_R map. For minimum power, the wing operates at an angle of attack of around 13 deg, and generates a lift of 450 lbs (out of a total of 550 lbs, or 82% lift share). Figure 22d shows the total section drag (Eq. 3) at the optimal operating point is close to the lowest values calculated. Returning to Fig. 22b, it is noted that at 80 kts, the wing is incapable of producing the entirety of the required 550 lbs lift. Even though the rotor is set at low 20 deg cant angle (predominantly in propeller mode), the combination of this cant angle and the ~13 deg wing angle of attack, results in more than half the rotor thrust contributing to the total lifting force. In addition, the rotor H-force also contributes to the total lifting force at levels comparable to the contribution of the rotor thrust.

Figure 23 and Figs. 24a–24d present a comprehensive set of results at 120 kts (high speed cruise). On Fig. 23, the minimum power point corresponds to a θ_R of 85 deg and a β of 0 deg (rotor oriented forward in propeller mode), consistent with the results previously seen on Figs. 18a and 18c. On Fig. 24a, the minimum power point corresponds to operation at minimum RPM values on the β– θ_R map. From Figs. 24b and 24c it is observed that for minimum power, the wing operates at an angle of attack of around 1.4 deg, and provides the entire 550 lbs lift. Operating optimally at zero cant angle and low wing angle of attack results in minimum section drag (Eq. 3), as seen in Fig. 24d. At 120 kts, if the rotor cant angle is increased so the rotor is now providing some lift, the wing angle of attack needs to correspondingly reduce (Fig. 24c) to reduce wing lift contribution (Fig. 24b). Since rotor-borne lift is energetically much more expensive than wing borne lift, total power requirements correspondingly increase with increasing rotor cant (Fig. 23). A similar analysis was conducted at a dash speed of 160 kts, and the results (not shown in the manuscript) were observed to be qualitatively similar to the 120 kts case discussed earlier in this paragraph. For minimum power, the rotor is canted entirely forward (in propeller mode), the rotor pitch is set very high (85 deg) to counter the large axial velocity. The wing provides the entirety of the 550 lbs lift, and does so at an even lower angle of attack at this higher speed.

Figure 25 shows minimum power versus flight speed for several values of fixed root pitch. Results for the variable pitch case (open circles on Fig. 25) previously seen in Fig. 17, are also included as a point of reference.

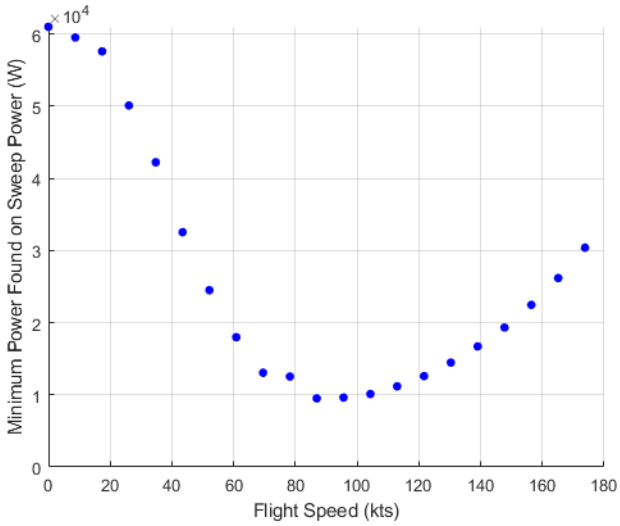

Fig. 17: Minimum rotor power vs flight speed

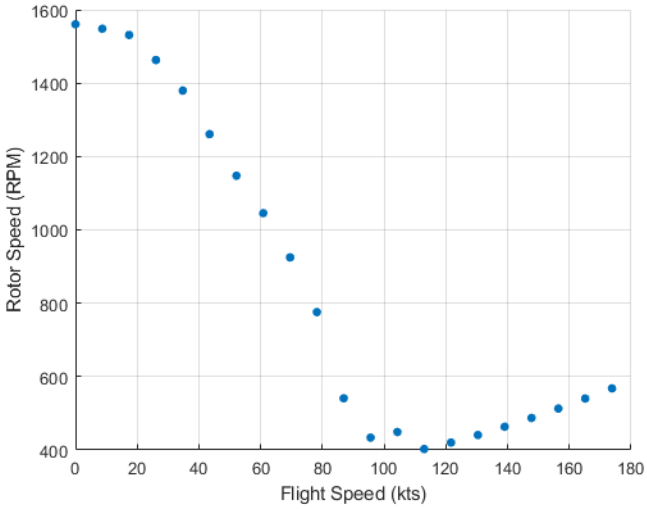

Fig. 18b: Rotor speed vs flight speed at minimum power

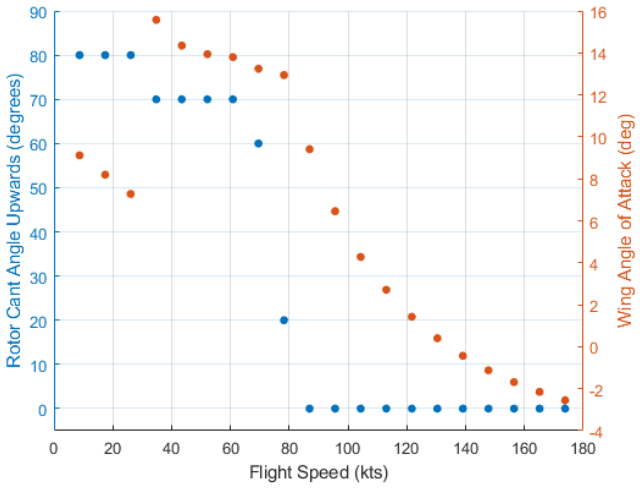

Fig. 18a: Rotor cant angle and wing angle of attack vs flight speed at minimum power

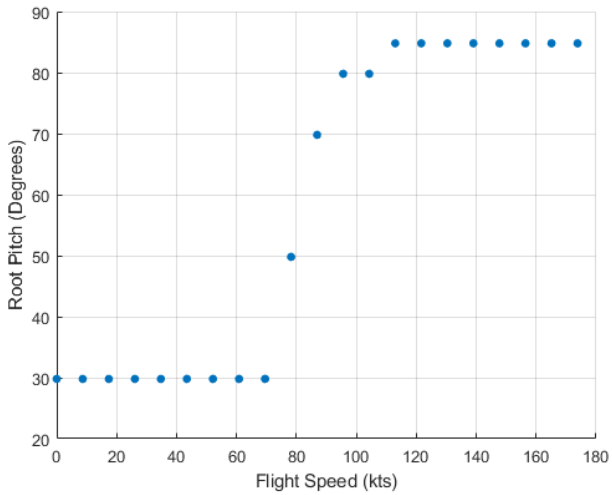

Fig. 18c: Rotor root pitch vs flight speed at minimum power

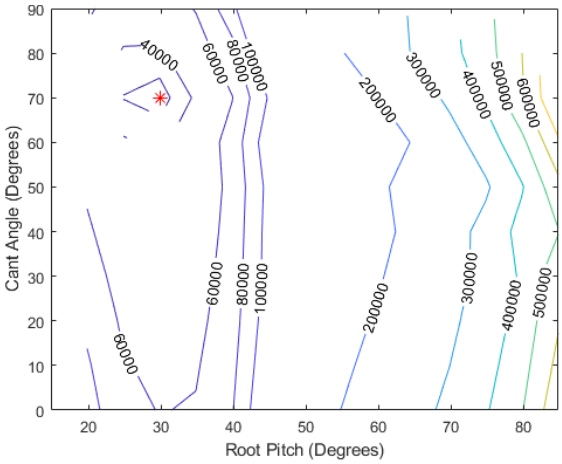

Fig. 19: Rotor power (W) with parametrically varied root pitch and rotor cant angle at 40 kts

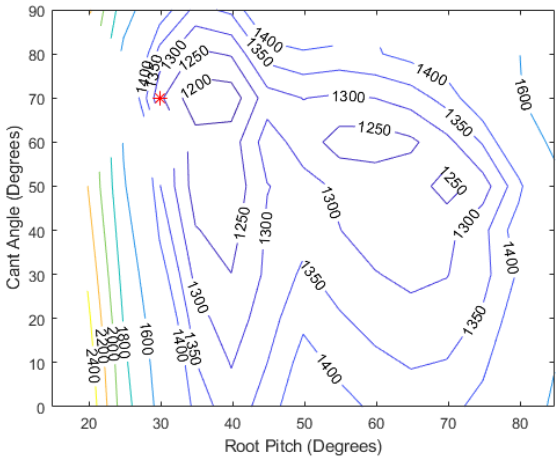

Fig. 20a: Rotor speed (RPM) with parametrically varied root pitch and rotor cant angle at 40 kts

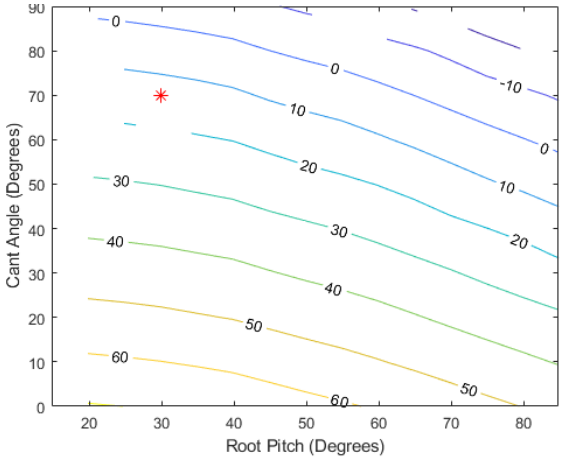

Fig. 20c: Wing angle of attack (deg) with parametrically varied root pitch and rotor cant angle at 40 kts

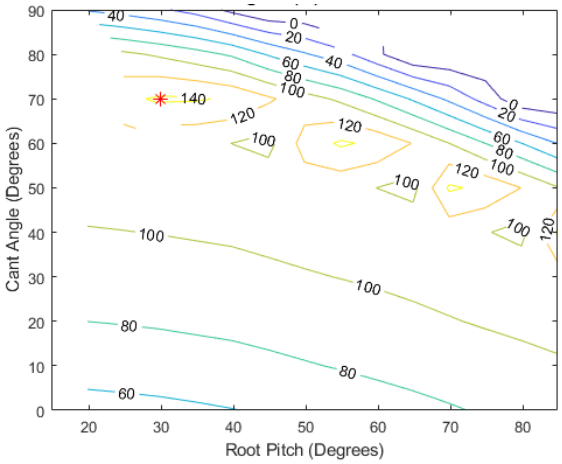

Fig. 20b: Wing lift (lb) with parametrically varied root pitch and rotor cant angle at 40 kts

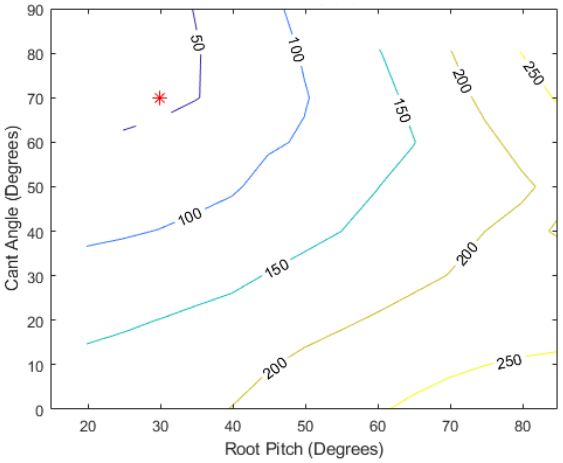

Fig. 20d: Section drag (lb) with parametrically varied root pitch and rotor cant angle at 40 kts

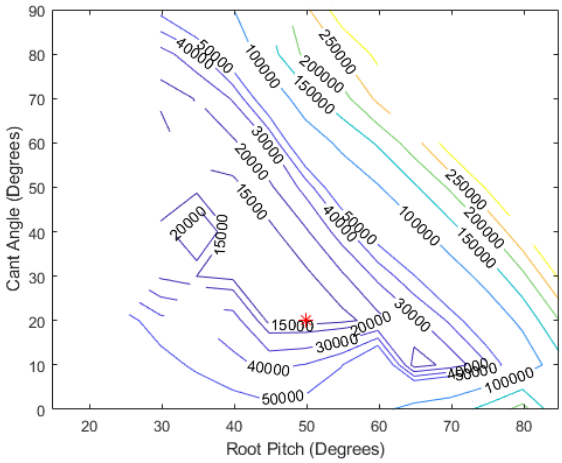

Fig. 21: Rotor power (W) with parametrically varied root pitch and rotor cant angle at 80 kts

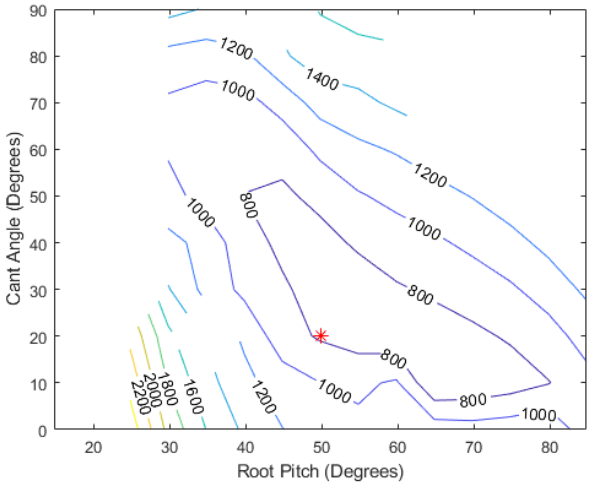

Fig. 22a: Rotor speed (RPM) with parametrically varied root pitch and rotor cant angle at 80 kts

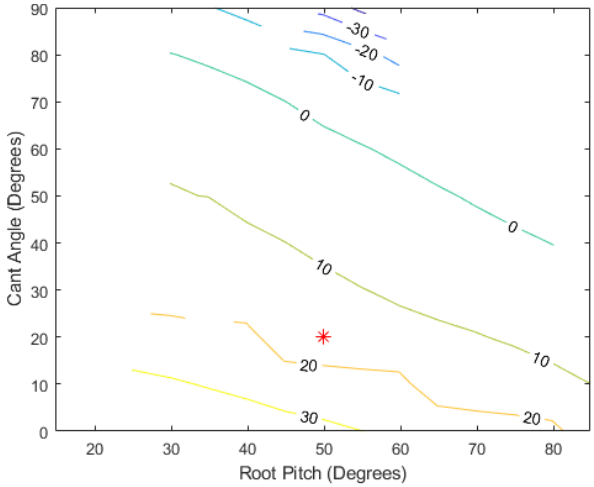

Fig. 22c: Wing angle of attack (deg) with parametrically varied root pitch and rotor cant angle at 80 kts

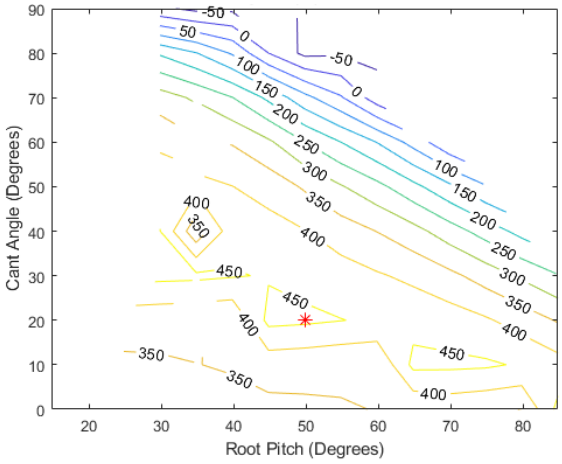

Fig. 22b: Wing lift (lb) with parametrically varied root pitch and rotor cant angle at 80 kts

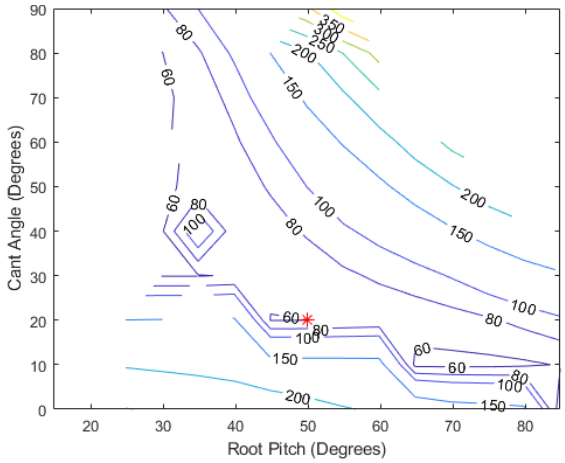

Fig. 22d: Section drag (lb) with parametrically varied root pitch and rotor cant angle at 80 kts

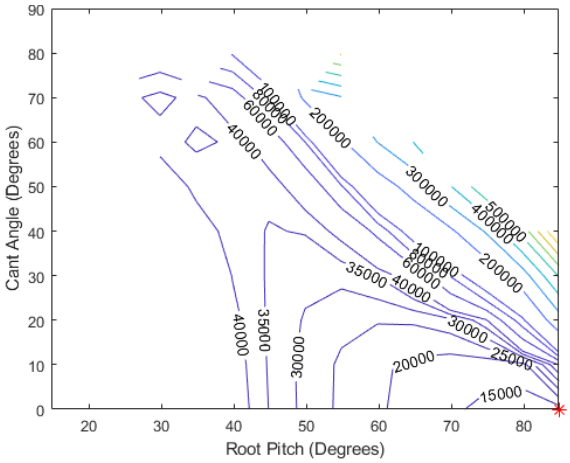

Fig. 23: Rotor power (W) with parametrically varied root pitch and rotor cant angle at 120 kts

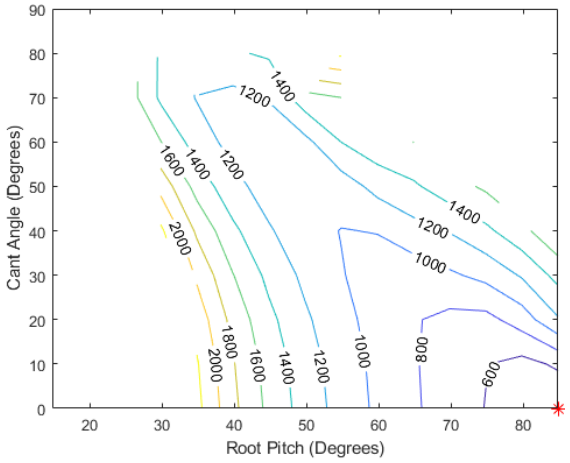

Fig. 24a: Rotor speed (RPM) with parametrically varied root pitch and rotor cant angle at 120 kts

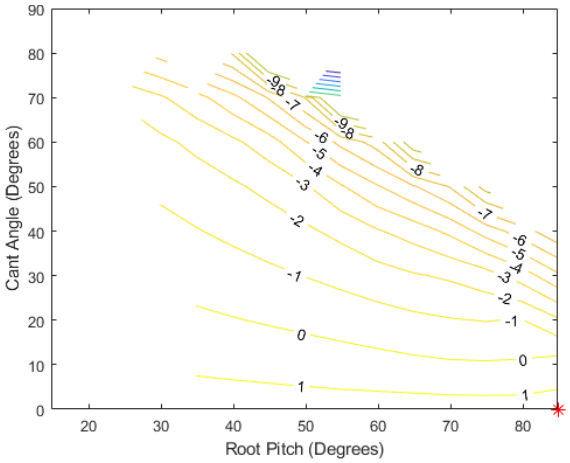

Fig. 24c: Wing angle of attack (deg) with parametrically varied root pitch and rotor cant angle at 120 kts

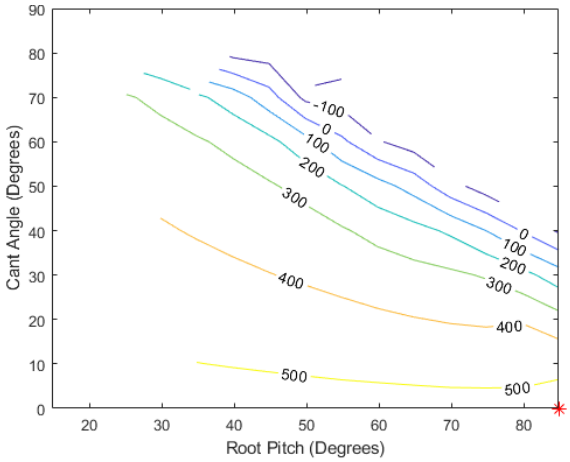

Fig. 24b: Wing lift (lb) with parametrically varied root pitch and rotor cant angle at 120 kts

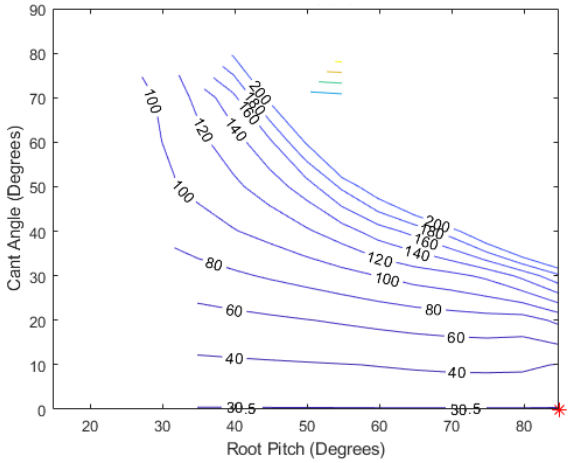

Fig. 24d: Section drag (lb) with parametrically varied root pitch and rotor cant angle at 120 kts

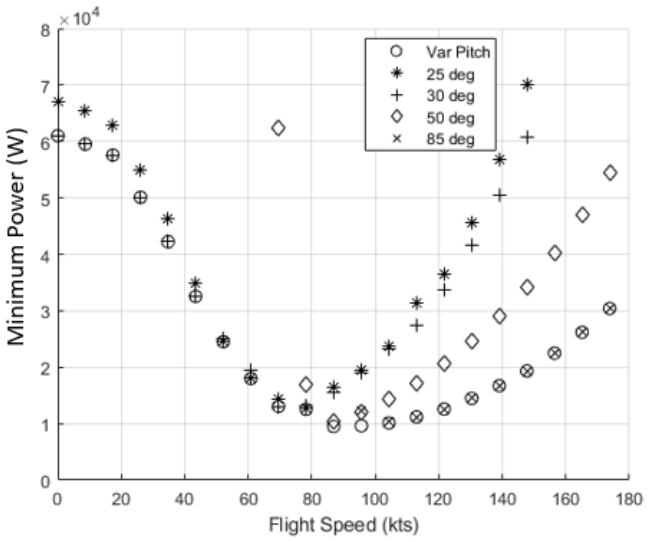

Fig. 25: Minimum power vs flight speed for fixed and variable pitched rotors

Recall that the corresponding optimal pitch variation was shown in Fig. 18c. From Fig. 18c the optimal pitch was 30 deg for speeds lower than 70 kts, and 85 deg for speeds above 110 kts, with the pitch increasing between these speeds. On Fig. 25 a fixed 30 deg root pitch ("plus" symbols) has identical power requirement to variable pitch case for speeds up to 70 kts (as expected), but the power requirement increases significantly at higher speeds. Higher rotor pitch settings are favored at higher speeds to account for the axial flow component through the rotor, but are detrimental at low speed as the rotor operates in stalled condition. For example, on Fig. 25, the power penalty at high speed with a fixed 50 deg root pitch (hollow diamond symbols) is a fraction of that corresponding to a fixed 30 deg root pitch, but at ~70 kts cruise speed the power is ~4.6 times higher than that with an optimal 30 deg root pitch, and this factor continues to increase as the cruise speed decreases further (results not shown on Fig. 25 for speeds below 70 kts as these would be off the scale). Similarly, on Fig. 25, while the power requirement for a fixed 85 deg root pitch ("cross" symbols) is minimum at speeds greater than 100 kts, the power requirements rise tremendously at lower speeds. At 80 kts, for example, the power requirements can be 10-15 times greater than the minimum power (results not shown on Fig. 25 as they would be off the scale) on account of the rotor being in deep stall. Using a lower fixed pitch than the optimal. Low-speed pitch below 30 deg (for example, a fixed root pitch of 25 deg) is worse than the 30 deg low-speed optimal pitch over the entire airspeed range.

For the 20 lbs aircraft in the previous section, it was observed that using a fixed rotor pitch that was optimal at low speed yielded a power penalty of only about 17–26% in moderate- to high-speed cruise. In contrast, for the 3,300 lbs aircraft in the present section, the power penalty in high-speed associated with the use of fixed rotor pitch that was optimal at low speed is ~4.6 times (compared to a variable pitch rotor whose pitch is set high, in high-speed cruise). This suggests that while a fixed pitch (optimal low-speed value) may be feasible for the 20 lbs vehicle, variable pitch might be unavoidable at the larger scale.

However, a key distinction in rotor solidity between the 20 lbs and 3,300 lbs vehicles considered in this study needs to be noted. For the 20 lbs vehicle, a low solidity of 0.06, typical of 2-bladed propellers on small UAS-scale Multicopter, was used. On the other hand, a much higher solidity of 0.265 more typical of UAM-scale eVTOL suitable for human transportation, is used for the 3,300 lbs vehicle. The 3,300 lbs aircraft, with rotor solidity reduced to 0.06 was also analyzed, for comparison. While a comprehensive set of results is not presented, Fig. 26 shows contours of power requirement at 120 kts, and a comparison to Fig. 23 shows that the optimal root pitch is around 60 deg (much closer to the 55 deg value for the 20 lbs aircraft at high speed, 35 kts, than the 85 deg value for the 3,300 lbs aircraft with the higher 0.265 solidity). Figure 27 shows minimum power requirement, versus root pitch, for the 3,300 lbs aircraft at 120 kts cruise, for the two different values of rotor solidity under consideration. It is seen that the high 0.265 solidity calls for a high rotor pitch setting (with the rotor operating in axial propeller mode), and a reduced pitch incurs a significant power penalty. Conversely, for the lower rotor solidity of 0.06, while the minimum power is at 60 deg root pitch, a reduced pitch of 30 deg results in only a small power penalty. From the above, using fixed pitch (for operation over a range of airspeeds) appears to be feasible on lower solidity rotors, and less so on higher solidity rotors, and is not necessarily related to aircraft scale (gross weight).

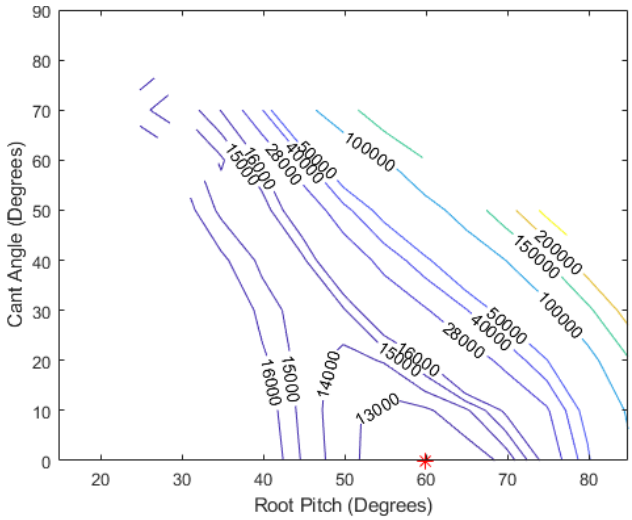

Fig. 26: Rotor power (W) with parametrically varied root pitch and rotor cant angle at 120 kts, low solidity ($\sigma = 0.06$)

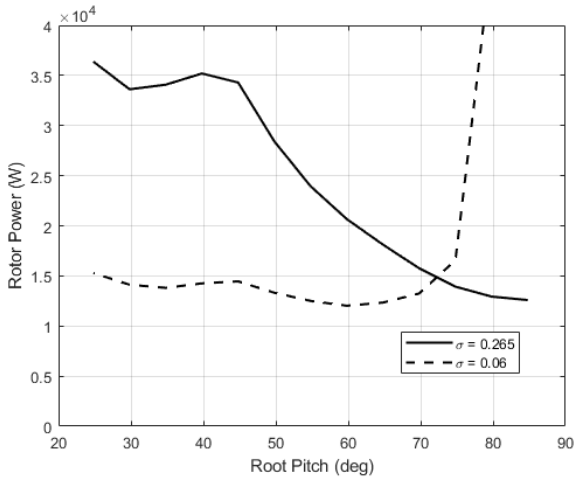

Fig. 27: Rotor power vs root pitch at low and high solidity

CONCLUSIONS

eVTOL aircraft with tilting rotors and fixed wings for cruise lift have control redundancy and can be operated optimally to minimize power requirement over the range of airspeeds. In this study, a single rotor-wing unit is considered to examine how a combination of rotor RPM, rotor root pitch, rotor cant (variable tilt between axial propeller and lifting rotor configurations) and wing angle of attack can minimize the power requirement, while ensuring that the rotor-wing unit provides the necessary lifting and propulsive forces.

At the UAV-scale, a rotor-wing unit providing 5 lbs lift was examined (notionally as one of 4 such units on a 20 lbs aircraft). For this case, the maximum endurance speed was 25 kts and the best range speed was between 25–30 kts. For minimum power operation, the rotor was oriented mostly upward (cant angle of 80 deg) up to a speed of 15 kts, and forward (cant angle of 0 deg) at speeds greater than 25 kts, with transition between 15–25 kts. At low speeds, when the rotor is primarily lifting, the root pitch is set relatively low (25 deg), and at high speed when the rotor is operating as an axial propeller, the root pitch is set high (60 deg), with the pitch increasing between these values over the 25–35 kts speed range. At 15 kts, the wing angle of attack was under 10 deg, and the wing lift share was 24%. At 25 kts (max endurance), with a wing angle of attack of around 12 deg, the wing lift-share increased to 83%. At 35 kts, the wing angle of attack was around 3 deg, and the wing provided almost the entire lift.

Instead of variable rotor pitch, a rotor with a fixed 25 deg pitch setting (optimal under 25 kts) is feasible for operation up to about 35 kts, albeit with an increase in required power. Over a 25-30 kts speed range, this rotor has an average 17% power penalty over a variable pitch rotor, and at 35 kts this increases to 26%. Using the 25 deg fixed pitch rotor requires the rotor cant angle to be high, implying that the rotor is oriented substantially upward and contributes ~28% of the total lift at 35 kts, as compared to the variable pitch case where the rotor is operating at zero cant as an axial propeller and the wing provides the entire lift.

At the manned-UAM scale, a rotor-wing unit providing 550 lbs lift was examined (notionally as one of 6 such units on a 3,300 lbs aircraft). For this case, the maximum endurance speed was 80–90 kts, and the best range was between 100–110 kts. For minimum power operation, the rotor was oriented mostly upward (cant angle of 70–80 deg) up to a speed of 60 kts, and forward (cant angle of 0 deg) at speeds greater than 80 kts, with transition between 60–80 kts. At low speeds, when the rotor is primarily lifting, the root pitch is set relatively low (30 deg), and at high speed when the rotor is generally operating as an axial propeller, the root pitch is set high (85 deg), with the pitch increasing between these values over the 70–110 kts speed range. At 40 kts the wing angle of attack is around 14 deg, and the wing lift share ~25%. At 80 kts wing angle of attack is ~13 deg and generates 82% of the lift share. At 120 kts the wing angle of attack of is around 1.4 deg, and provides all of the lift requirement. These observations are qualitatively similar to those made at the UAV-scale.

Differing from the UAV-scale, a 30 deg fixed pitch rotor (optimal at speeds below 70 kts) does not appear to be feasible at moderate to high speeds as the power penalty becomes too steep. On closer examination, though, this limitation was found to be related to the much higher rotor solidity at the manned-UAM scale. If the rotor solidity is reduced to values comparable to the UAV-scale rotor, then a fixed pitch setting again appears to be feasible over the entire flight speed range.

Author contact: Jonah Whitt whittj4@rpi.edu
Dr. Farhan Gandhi gandhf@rpi.edu.

REFERENCES

1. "Joby Aviation S4," https://evtol.news/joby-s4, accessed October 21, 2022.
2. "Archer Midnight (production aircraft)," https://evtol.news/archer, accessed October 21, 2022.
3. "Wisk Aero Generation 6," https://evtol.news/wisk-aero-generation-6, accessed October 21, 2022.
4. "Wisk Aero Cora (Generation 5)" https://evtol.news/kitty-hawk-cora/, accessed October 21, 2022.
5. "Vertical Aerospace VA-X2 (prototype)," https://evtol.news/vertical-aerospace-seraph/, accessed October 21, 2022.
6. https://vertical-aerospace.com/vx4/, accessed October 21, 2022.
7. https://en.wikipedia.org/wiki/Boeing_Passenger_Air_Vehicle, accessed October 21, 2022.
8. https://www.boeing.com/features/highlights/2020/cargo-air-vehicle/index.page, accessed October 21, 2022.

9. “Beta Technologies ALIA,” https://evtol.news/beta-technologies-alia/, accessed October 21, 2022.

10. “EHang 216,” https://evtol.news/ehang-216/, accessed October 21, 2022.

11. “EHang 184 (defunct),” https://evtol.news/ehang/, accessed October 21, 2022.

12. Reddinger, J.-P., and Gandhi, F., “Physics-Based Trim Optimization of an Articulated Slowed-Rotor Compound Helicopter in High-Speed Flight,” J. of Aircraft, Vol. 52, No. 6 (2015), pp. 1756-1766. doi: 10.2514/1.C032939.

13. Reddinger, J.-P., Gandhi, F., and Kang, H., “Using Control Redundancy for Power and Vibration Reduction on a Compound Helicopter at High Speeds,” Journal of the American Helicopter Society, Volume 63, Number 3, July 2018, pp. 1-13(13), **DOI:** 10.4050/JAHS.63.032009.

14. Jacobellis, G., Gandhi, F., and Floros, M., “Using Control Redundancy for Power and Vibration Reduction on a Coaxial Rotor Helicopter at High Speeds,” J. of the American Helicopter Society, Vol. 64, No. 3, July 2019. https://doi.org/10.4050/JAHS.64.032008.

15. Barron, H. M., Brentner, K., Hornand, J. F., Ozdemir, G., and Throsen, A., “Acoustic Analysis of Compound Helicopters with Trim Variations,” American Helicopter Society 69th Annual Forum, Phoenix, AZ, May 21–23, 2013.

16. Reddinger, J.-P., McIntosh, K., Zhao, D., and Mishra, S., “Modeling and Trajectory Control of a Transitioning Quadrotor Biplane Tailsitter,” Vertical Flight Society 75th Annual Forum Proceedings, May 2019.

17. Silva, C., Johnson, W., Antcliff, K. R, and Patterson, M. D., “VTOL Urbain Air Mobility Concept Vehicles for Technology Development,” AIAA Aviation and Aeronautics Forum, 2018.

18. Niemiec, R., and Gandhi, F., “The Rensselaer Multicopter Analysis Code (RMAC): A Physics-Based Comprehensive Modeling Tool,” Vertical Flight Society 75th Annual Forum Proceedings, May 2019.

19. Anderson, J., *Fundamentals of Aerodynamics*, 6th ed., McGraw Hill Education, 2017. Chapter 5.